Subaqueous dilative slope failure (breaching): Current understanding and future prospects

Alhaddad, S.M.S.; Keetels, G.H.; Mastbergen, Dick ; van Rhee, C.; Lee, Cheng-Hsien; Montellà, Eduard Puig; Chauchat, Julien

DOI
10.1016/j.advwatres.2024.104708

Publication date
2024

Document Version
Final published version

Published in
Advances in Water Resources

Citation (APA)
Alhaddad, S. M. S., Keetels, G. H., Mastbergen, D., van Rhee, C., Lee, C.-H., Montellà, E. P., & Chauchat, J. (2024). Subaqueous dilative slope failure (breaching): Current understanding and future prospects. *Advances in Water Resources*, *188*, Article 104708. https://doi.org/10.1016/j.advwatres.2024.104708

Advances in Water Resources 188 (2024) 104708

Contents lists available at ScienceDirect

Advances in Water Resources

journal homepage: www.elsevier.com/locate/advwatres

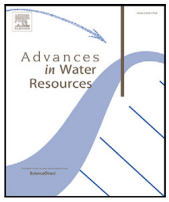

Review

Subaqueous dilative slope failure (breaching): Current understanding and future prospects

Said Alhaddad [a,*], Geert Keetels [a], Dick Mastbergen [b], Cees van Rhee [a], Cheng-Hsien Lee [c], Eduard Puig Montellà [d], Julien Chauchat [d]

[a] Offshore and Dredging Engineering, Delft University of Technology, Leeghwaterstraat, Delft, 2628 CN, The Netherlands
[b] Department of Marine and Coastal Management, Deltares, Boussinesqweg 1, Delft, 2629 HV, The Netherlands
[c] Department of Marine Environment and Engineering, National Sun Yat-sen University, Kaohsiung, 80424, Taiwan
[d] LEGI, Université Grenoble Alpes, Grenoble, 38000, France

ARTICLE INFO

Keywords:
Breaching
Flow slides
Sand erosion
Turbidity currents
Underwater slope failure

ABSTRACT

This article presents the current state-of-the-art understanding of underwater dilative slope failure (breaching). Experimental investigations are reviewed, providing critical insights into the underlying physics of breaching and pointing out knowledge gaps, which underscore the need for further research. Besides, field observations at several locations across the globe are outlined, highlighting the hazard of breaching and the need for effective coastal management strategies to mitigate the associated risks. Furthermore, existing methods for analyzing and predicting the slope failure evolution are discussed and reflected upon, including analytical approaches and numerical models, ranging from simplified 1D models to advanced 3D coupled flow-soil approaches. Lastly, open questions are posed and key future directions are identified to enhance our understanding of the breaching failure. Overall, this review paper provides a valuable resource for researchers and decision makers involved in slope stability and flow slide risk assessment.

1. Introduction

Slope failures are ubiquitous in both subaerial and subaqueous environments, causing serious damage all over the globe. Therefore, the subject of slope failures receives increased attention of researchers across a wide range of scientific fields, such as soil mechanics, natural hazards, sedimentology, dredging, and hydraulic engineering.

This article is concerned with a specific type of underwater slope failures, during which the sediment forming the slope shows a dilative behavior. Hereafter, 'breaching' is used as an abbreviated term for this subaqueous dilative slope failure. Our objectives are to provide a better insight into the physics of breaching, identify principle knowledge gaps, and provide a prospective pathway to tackle the future research challenges. Section 1.1 first presents a detailed explanation of breaching. Following that, the significance of understanding breaching is the focus of Section 1.2 and the initiation mechanisms of breaching are the focus of Section 1.3.

1.1. Nature of breaching

In hydraulic engineering, the term 'breaching' usually refers to the ultimate failure caused by the overtopping of dikes, dams, embankments, and sand barriers (Eke et al., 2011). However, in the context of submerged slope failures, this term has been used in the literature to describe a more specific phenomenon. To avoid conceptual and nomenclatural problems, breaching is specifically defined here as slow (~mm/s), gradual, retrogressive erosion of submerged slopes that are steeper than the internal friction angle of the granular material forming that slope (Van den Berg et al., 2002).

For long time, breaching was overlooked by researchers, because it was confused with soil liquefaction, which is a phenomenon wherein an abrupt collapse of the soil structure occurs due to an increase in pore water pressure. This confusion resulted in inaccurate interpretation of the process behind many slope failures, and arose from the comparable post-event morphologies produced by both failures (Van den Ham et al., 2014); in the past, only post-event morphology was available, which

* Corresponding author.
E-mail addresses: S.M.S.Alhaddad@tudelft.nl (S. Alhaddad), G.H.Keetels@tudelft.nl (G. Keetels), Dick.Mastbergen@deltares.nl (D. Mastbergen), C.vanRhee@tudelft.nl (C. van Rhee), Kethenlee@mail.nsysu.edu.tw (C.-H. Lee), Eduard.Puig-Montella@univ-grenoble-alpes.fr (E. Puig Montellà), Julien.chauchat@univ-grenoble-alpes.fr (J. Chauchat).

https://doi.org/10.1016/j.advwatres.2024.104708
Received 10 August 2023; Received in revised form 4 March 2024; Accepted 18 April 2024
Available online 23 April 2024

was insufficient to determine the mechanism behind the observed failures. Recent field observations and laboratory tests have, nonetheless, demonstrated that the primary failure mechanism in underwater slopes composed of fine sand is breaching (Mastbergen et al., 2016; Van den Berg et al., 2017; Mastbergen et al., 2019). The term 'flow slide' is popularly encountered in the literature as the overarching term for both failure mechanisms: liquefaction and breaching.

Breaching has remained unexplored until it was brought to the light by the Dutch dredging industry in the 1970s as an efficient production mechanism for stationary suction dredgers. In this respect, it is also worth noting that breaching occurs during a number of dredging activities, explaining why a large part of the contemporary knowledge pertaining to this phenomenon comes from dredging research (e.g., Breusers (1977), Van Rhee and Bezuijen (1998)).

Breaching is predominantly encountered in moderately to densely-packed (relative density = 50%–90%) fine sands (grain size = 100–200 μm) (Van Rhee and Bezuijen, 1998; Van Rhee, 2015), which undergoes dilation under the influence of shear forces. The dilative behavior of such sediment results in pore space increments, producing a negative pore pressure with respect to the ambient pressure. This phenomenon, reported by Iverson et al. (1997) and termed pore pressure feedback, is responsible for the increment of shear strength, which substantially impedes the process of erosion (Van Rhee, 2010). As a result of the pressure difference, an inward hydraulic gradient arises, forcing the ambient water to infiltrate into the sand pores, thereby dissipating the negative pressure (Alhaddad et al., 2019). Consequently, sand particles located at the sand-water interface lose their stability and detach sequentially from the slope surface (or 'breach face') (Alhaddad et al., 2020c). While falling down, these particles mix with the surrounding water, producing a sustained turbidity current that travels along the breach face and subsequently progresses down the slope toe (Van Rhee and Bezuijen, 1998; Eke et al., 2011; Alhaddad et al., 2020c) (see Fig. 1). This current exerts an additional shear stress upon the slope surface, consequently increasing the sediment erosion rate. Through large-scale experiments, Alhaddad et al. (2020c) found out that breaching-generated turbidity currents are self-accelerating along the breach face; the current accelerates itself by the accumulated erosion of sediment from the breach face.

At the base of the slope surface, the turbidity current impinges on the bed and makes a sharp turn, and then runs down over the downstream region (Eke et al., 2011; Alhaddad et al., 2020c). A hydraulic jump may occur somewhere at the transition between the breach face and the downstream region, resulting in a scour pit, where energy of the flow is partially dissipated. To the best of our knowledge, no research has focused on this transition, leaving our understanding of the interaction between the flow and slope toe limited. Based on prior experimental observations (Van Rhee and Bezuijen, 1998), it has been established that breaching can be characterized by two distinct failure modes: stabilizing and destabilizing (Fig. 2). Breaching is classified as stabilizing when the height of the breach face gradually reduces over time until it completely vanishes. Conversely, during destabilizing breaching, the height of the breach face progressively increases over time, ultimately leading to an uncontrolled and retrogressive failure of the slope. In both cases, the failure stops when the sediment morphology reaches an angle milder than or near the internal friction angle.

The impact of the breaching-generated turbidity current mainly governs whether the breaching process is stabilizing or destabilizing (Van Rhee, 2015). When sediment is deposited by the turbidity current at the breach face toe, the breach height will steadily diminish and ultimately vanish. Conversely, if the turbidity current erodes sediment at the breach face toe, the breach height will increase over time, causing destabilizing breaching. In practice, destabilizing breaching might continue until the entire sand body is eroded.

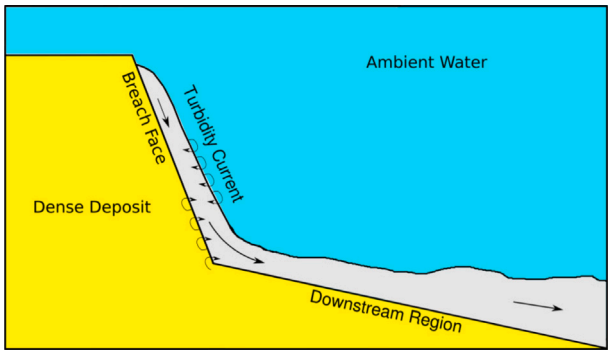

Fig. 1. Schematic representation of breaching and the accompanying turbidity currents (modified from Alhaddad et al. (2021)).

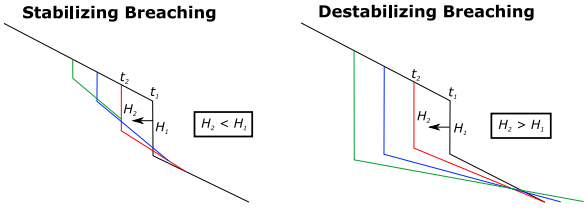

Fig. 2. Diagrammatic illustration of the temporal evolution of failure during stabilizing breaching (**left**) and destabilizing breaching (**right**); H is the breach height and t is time, where H_1 and H_2 correspond to t_1 and t_2, respectively. The arrows indicate the direction of erosion.

1.2. Significance of breaching

Breaching can occur in naturally-deposited fine sands in estuaries, along riverbanks, shoals, beaches and in artificial sand fill. This process has both beneficial and hazardous aspects. For example, in dredging operations breaching is created intentionally to promote sand production (e.g., in mining pits (Alhaddad and Elerian, 2024) and during the operation of cutter suction dredgers). During flushing operations of reservoirs, breaching can be used to promote sediment transport downstream of dams. On the other hand, breaching can start naturally or unintentionally during dredging operations and progress in an uncontrolled way, which can threaten the stability of the foundation of submarine and near-shore infrastructure, including levees. This implies that breaching poses a threat to coastal habitation on a regional or even national level. In this respect, breaching deserves more recognition as an important type of geological hazard.

In the Netherlands, a manual for safe dredging planning and operation is in effect to prevent bank collapses during sand mining. In many parts of the world, however, sand mining is not well organized and may cause serious effects on the environment and residents. Fig. 3 shows the consequence of uncontrolled sand mining in the Mekong River, Vietnam (National-Geographic, 2018).

To gain a better overview of the risks associated with breaching, it is beneficial to reconsider the well-documented history of the Dutch south-western delta system. In the province of Zeeland in the south-west of the Netherlands, already before the 17th century, much land was reclaimed from the North Sea, like Vlietepolder at the island of Noord-Beveland (see Fig. 4). However, in the 18th and 19th centuries, the tidal currents in the Eastern Scheldt increased in strength. Much effort was made to design and build defence measures to protect the riverbanks, but often in vain. Coastal erosion and dike collapses resulted in flooding and much land was lost again. New dikes were constructed behind the old ones and the coastline had to be retreated periodically, resulting in the typical shape of today. The events, called bank falls, were accurately monitored and described in Dutch publications of the 19th century and can be identified now as slowly retrogressing breaching flow slides (Mastbergen et al., 2019).

Fig. 3. Bank collapses at Mekong River, Vietnam, due to uncontrolled sand mining resulting in breaching (National Geographic, 2018, photo: Sim Chi Yin). Breaching scars are indicated with red dashed lines.

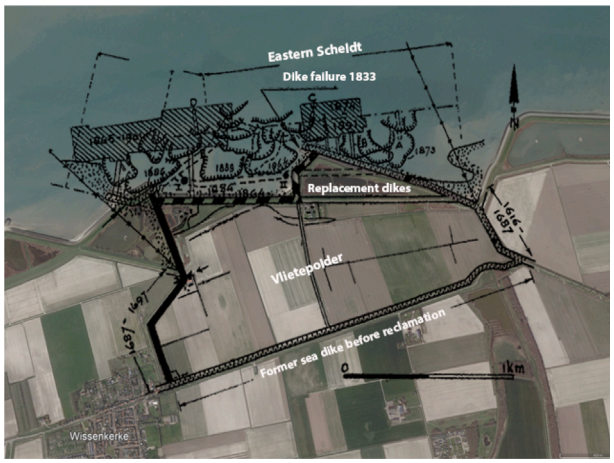

Fig. 4. Flow slides in the 19th century in Vlietepolder, Noord-Beveland, the Netherlands. Overlay view of historic development in 1670–1890 with observed flow slides (De Bruin and Wilderom, 1961) and present situation (Google Maps, 2023). The remains of damaged and new dikes are clearly visible, resulting in the typical coast shape.

Only in the late 20th century, with the Delta Works, all coastlines in Zeeland were finally adequately protected. Since then, there have been no further dike collapses and live events were not observed anymore. Currently, legislation is in place to design and monitor primary levees using a failure probability assessment to prevent future collapses and flooding. The risk assessment method considers various modes of slope failure including breaching (Van den Ham et al., 2014).

A storm surge barrier was built in the Eastern Scheldt, with a bed protection layer to prevent scour and flow slides. As part of the maintenance plan, the bathymetry in the neighboring region at the end of this protection layer was closely monitored on a yearly basis. A differential bathymetry analysis revealed a number of so far unnoticed large flow slides that took place completely under water in the side slopes (Mastbergen et al., 2019). Moreover, shoal margin collapses still occur frequently and can be detected in yearly differential bathymetry maps (Van Dijk et al., 2018).

In the Brahmaputra–Jamuna delta in Bangladesh, the current situation is comparable with that in the Netherlands in the 19th century (i.e., land reclamation resulting in increased tidal currents, poor protection with increasing coastal erosion and flow slides, threatening infrastructure and even the city of Sirajganj). Efforts to protect the banks were reported by Van der Wal (2020).

Several mitigation measures have been developed to limit the adverse impact of breaching (Mastbergen et al., 2019): sand nourishment, installation of rock and permeable geotextile on the top of sand beds, the application of rock-enforced mattresses and installation of stone walls at shore lines. Nonetheless, these methods are expensive, work partially, and require continues monitoring and subsequent interventions after installation in regions prone to breaching.

In the light of the aforementioned observations, it is evident that it is crucial to assess the risks associated with breaching and define appropriate mitigation measures to prevent loss of land, flooding and damage to submarine and near-shore infrastructure.

1.3. Triggering mechanisms

Any mechanism that results in an underwater slope of a moderately/densely-packed sediment being steeper than the internal friction angle is regarded as a triggering mechanism of breaching. For instance, gradual increase in the steepness of submerged slopes due to erosion processes caused by river or tidal currents in estuaries can potentially trigger breaching events. Additionally, scouring at the toe of submerged slopes may also trigger breaching by causing the slope to become over-steepened and thus unstable; once the slope angle surpasses the internal friction angle, retrogressive erosion occurs, starting at the toe of the slope. The Mississippi riverbank is a notable example of such retrogressive failures that reached close to levees and nearby industrial areas, and has been well-documented in the literature (Torrey, 1988).

It should be noted that our understanding of the mechanisms that trigger breaching events is currently very limited, indicating a need for further investigation and research in this area. For instance, breaching events at Amity Point in Queensland, Australia, continue to be observed without a clear understanding of their triggering mechanism (Beinssen et al., 2014; Brilli et al., 2019), although the physics of the breaching process is now well understood.

2. Experimental data and field observations

In Section 2.1, we provide an overview of the breaching laboratory experiments reported in the literature and we reflect on the experimental observations. Following that, in Section 2.2, we discuss recent field observations, shedding light on the knowledge obtained from them.

2.1. Laboratory experiments

Due to the unpredictable nature of breaching events in field situations and the potential for turbidity currents to damage measuring instruments, it is quite challenging to obtain controlled *in situ* measurements of breaching. As a result, the vast majority of the existing knowledge on breaching comes from laboratory studies.

The very first breaching laboratory experiments reported in the literature are those of Van Rhee and Bezuijen (1998), where it was concluded that turbidity currents play an important role in breaching. In addition to the grain-by-grain erosion, intermittent collapses of coherent sand wedges, referred to as surficial slides, were observed in these experiments. Here, it was also recognized for the first time that the breaching failure could be stabilizing or destabilizing. One decade later, Eke et al. (2009) conducted laboratory experiments and collected measurements for the turbidity currents traveling down the toe of the breach face. You et al. (2012) also conducted laboratory experiments focusing on the soil mechanical aspects of breaching and termed the variant that involves grain-by-grain failure and surficial slides as ‘dual-mode slope failure’. However, Van den Berg et al. (2017) disagreed with this terminology, arguing that grain-by-grain failure and surficial slides are inherent properties of breaching and are closely linked. During grain-by-grain failure, the negative excess pore pressure dissipates locally, weakening the deposit near the sand-water interface, eventually leading to a thin surficial slide. This slide causes unloading

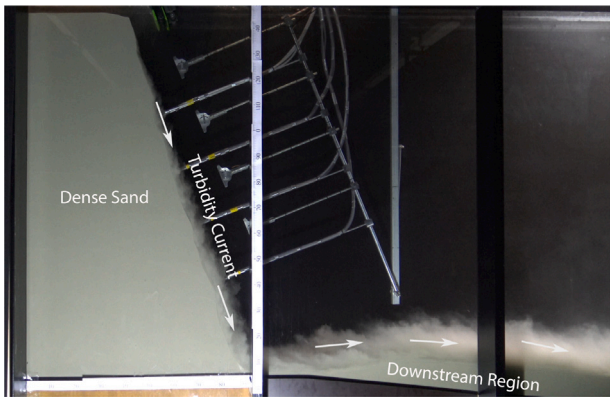

Fig. 5. A breaching experiment in progress; the initial angle of the breach face was 70° (Alhaddad et al., 2020c).

and a decrease in pore pressure, strengthening the deposit and reverting the slope failure process back to the grain-by-grain mode. We also adopt this argument and emphasize that this failure is breaching and not another type of failure; the authors witnessed and observed the occurrence of surficial slides in all breaching experiments.

A series of large-scale experiments (breach face length = 1.4–1.6 m, D_{50} = 135 μm) was carried out by Alhaddad et al. (2020c) in which various non-vertical initial slope angles were tested (see Fig. 5), delivering coeval direct measurements of the morphology evolution and the breaching-generated turbidity currents traveling over the breach face. In these experiments, the breaching failure was triggered by removing a confining wall that initially prevented the failure of the over-steepened homogeneous sand deposit. The failure mode was found to be stabilizing, and the obtained measurements demonstrated the development of the flow while visualizing the structure of its velocity and sediment concentration. Dense basal layers with high near-bed concentrations up to 0.5 by volume were observed, demonstrating the complexity of the dynamics of the bottom boundary layer of the flow, where the particle–particle and particle–fluid interactions affect the momentum and mass exchanges between the turbidity current and the breach face.

Alhaddad et al. (2020c) also explored the occurrence of surficial slides and found the following. Due to the difference in erosion rates along the breach face, with the lower part eroding faster than the upper part, a sediment overhang forms at the uppermost part of the breach face. The underpressure within the pores holds the sand particles together, allowing the formation of such an overhang. Eventually, the overhang collapses and slides downslope under the pull of gravity. It should be noted that this explanation holds for densely-packed sediment. In moderately-packed sand, the reason behind the occurrence of surficial slides remains poorly understood.

To investigate the failure mode of breaching (i.e., stabilizing or destabilizing), Alhaddad et al. (2023) executed a set of large-scale laboratory experiments, where both modes were observed. A common pronounced observation in the experiments of Alhaddad et al. (2020c) (flume width = 22 cm) and Alhaddad et al. (2023) (flume width = 50 cm) is that the erosion velocity of the breach face is non-uniform across the breach face width, resulting in a concave breach face. In other words, the breach face was inwardly curved in the erosion direction (see Fig. 6), regardless of the flume width. This erosion behavior seems to be an intrinsic property of the breaching problem; the ultimate morphology of breaching events documented in the literature also takes a concave shape (e.g., Mastbergen et al., 2019), (see Section 2.2). This implies that the breaching problem is three-dimensional.

Interestingly, both the experiments carried out by Alhaddad et al. (2020c, 2023) consistently revealed that breaching can trigger liquefaction. The sediment particles falling from the breach face deposit on the

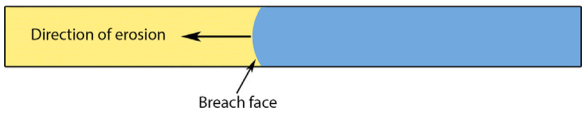

Fig. 6. Sketch of the top view of the sand deposit during breaching, as observed in laboratory experiments (Alhaddad et al., 2020c, 2023), showing the concavity of the breach face.

downstream region, creating a very loosely-packed sloping bed. Due to the accumulation of particles, the inclination of this bed gradually increases until reaching a critical angle beyond which the downstream region liquefies, resulting in a slurry-like flow.

Digital video cameras were commonly used in all aforementioned experiments to investigate the overall slope failure evolution and to measure the erosion rate along the breach face. Eke et al. (2009) utilized the video recordings to retrieve turbidity current thicknesses and velocities, while Alhaddad et al. (2020c) used ultrasonic velocity profilers (UVP) and obtained high-resolution velocity fields. Additionally, they combined three techniques (conductivity, UVP backscatter and siphon measurements) to obtain wall-normal sediment concentration profiles of turbidity currents.

2.2. Field observations

Laboratory experiments do not provide insights into all aspects of the process, due to the limited scale of facilities. Besides, field observations are relatively scarce, especially for active breaching events. However, amateurs or fellow researchers, who could be completely unaware of the breaching phenomenon, may still report interesting field observations or post photos and videos of breaching failures on the internet (e.g., those reported in Mastbergen et al. (2019)). In this section, a few examples of slope and bank collapses will be described, which show the typical characteristics of an active breaching event:

1. the slow retrogression speed (a few mm/s or m/hour), noticed when the breach face reaches the shoreline,
2. the typical amphitheatre-shaped crater,
3. the continuous falling of sand lumps into water when reaching the shore, and
4. the underwater almost-vertical breach face (6–10 m high) that does not collapse abruptly.

In 2014, the Flood Control Test was performed at the shoal of Walsoorden, in the Western Scheldt, the Netherlands, (Mastbergen et al., 2016). The test aimed at triggering and monitoring an active flow slide event. Multibeam surveying revealed the slow retrogression of 6 m steep breach faces during 2.5 h over 20 m. Only three months before the test was scheduled, a very large natural shoal margin collapse occurred at this location, retrogressing 300 m into the shore, with a volume of almost 1 Million m^3 (Van den Berg et al., 2017). Typical breaching features were observed, like the slow incision of gullies into the shoal, but unfortunately no detailed measurements were obtained, only multibeam surveys before and after the event. The field test was performed anyway a few hundreds of meters further along the shoal margin, with almost identical conditions. Why the small breaching events, triggered during the test by dredging, did not retrogress that far into the shore as the natural breaching event did, is discussed in Van den Ham et al. (2022). Their study suggests that the occurrence of liquefaction in deposits of very loosely-packed sand at the shoal margin may have significantly enhanced the natural breaching process, whereas no liquefaction occurred during the field test.

Meanwhile in Amity Point, Australia, frequent beach collapses were reported by Beinssen et al. (2014). Videos of these events matched exactly with the original eyewitness descriptions of flow slides in the Dutch reports of the 19th century.

Fig. 7. Beach collapse in Candelaria- Zambales, Philippines, 2013 (photo courtesy of Mines and Geosciences Bureau, Manila).

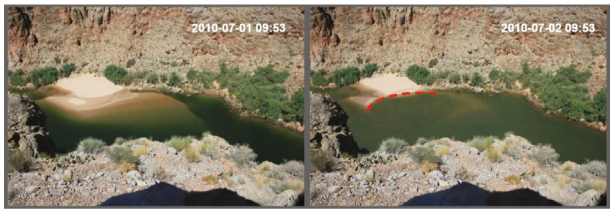

Fig. 8. Sand bar collapse in Colorado river, Grand Canyon, USA, (Lima, 2021). Breaching scar is indicated with the red dashed line. Event took place apparently between July 1-2, 2010.

Beach collapse, as a type of retrogressive breaching failure, occurs in many other parts of the world, but they often go unrecognized as breaching, as was the case in Zambales, Philippines. Various reports can be found on the news channels (e.g., ABS-CBN-News, 2013), see Fig. 7.

At Cap Ferret, France, special time-lapse cameras were installed to observe the evolution of frequently occurring flow slides, showing again the slow, amphitheatre-shaped retrogression into the beach (Nédélec et al., 2022). Additionally, in the Colorado river, Grand Canyon, USA, during dam flushing events, sand bars were observed with web cameras, showing evidence of flow slides, very similar to the observed beach collapses with amphitheatre-shaped retrogression in the sand bar and steep underwater slopes, as reported by Lima (2021), see Fig. 8.

In the Wadden Sea, in the north of the Netherlands, at the barrier islands Ameland and Vlieland, frequent beach collapses occur near coastal protection works (see Figs. 9 and 10, note that these figures depict the situation shortly after the failure event). These collapses take place periodically in these locations, near the existing bed protection and between the groynes that prevent further coastal erosion. The sand nourishment operations applied for mitigating erosion seem not very effective here, since the tidal current is deep and strong.

In summary, all above observed active events exhibit typical breaching characteristics, as opposed to shear or liquefaction slope failures, such as a slow retrogression speed. The events lasted from several hours to a full day. Another typical observation indicating the mechanism of breaching is the steep scarp above and under water. This is only possible in an active event due to the generation of pore-water suction. As soon as the event stops, the pore-water underpressures dissipate and the underwater slope reduces to the internal friction angle. Owing to the action of waves and currents, this slope will further disintegrate.

Fig. 9. Photograph of a beach collapse event that occurred at Ameland SW, the Netherlands, on December 28th, 2022 (Omrop Fryslan). The event was not active anymore when the photo was taken.

Fig. 10. Beach collapse at Oost-Vlieland between two groynes on January 5th, 2023; post-failure bathymetry (top), photo showing damaged dune foot (Rijkswaterstaat) (bottom). Breaching scar is indicated with the red dashed line.

3. Simplified analytical models

3.1. Wall velocity

Breusers (1977) coined the term 'wall velocity', which refers to the horizontal traveling speed of a submerged, vertical slope as a result of breaching. The formula for calculating the wall velocity can be obtained by balancing the various forces exerted on a particle located on a

slope (for a comprehensive derivation, the reader may refer to Van der Schrieck (2012)). The wall velocity, v_w [m/s], reads

$$v_w = \frac{\sin(\alpha-\phi)}{\sin\phi}\,\frac{(1-n_0)}{\delta n}k_l\,\frac{\rho_s-\rho_w}{\rho_w}, \tag{1}$$

where ϕ is the internal friction angle, α [°] is the slope angle, n_0 [-] is the *in situ* porosity of sand, k_l [m/s] is the sediment hydraulic conductivity at the loose state (at maximum porosity), ρ_s [kg/m^3] is the sediment density, ρ_w [kg/m^3] is the water density, and $\delta n = (n_l - n_0)/(1-n_l)$ is the relative change in porosity, in which n_l [-] is the maximum porosity of the sand. It is worth noting that Eq. (1) is valid only when $\alpha > \phi$, since breaching does not occur if $\alpha < \phi$.

Although sediment erosion rate can readily be calculated using Eq. (1), it is a greatly simplified approach, which does not include key physical processes. Neither the effect of turbidity currents nor the surficial slides is included in this formula, rendering unreliable results. Van Rhee and Bezuijen (1998) and Alhaddad et al. (2020c), for instance, found that this formula was invalid for their large-scale experiments. Besides, Alhaddad et al. (2020c) showed that Eq. (1) overestimates the grain-by-grain erosion at the top of the breach face, where turbidity currents are not erosive, by 18%–96%.

Furthermore, the use of the hydraulic conductivity at the loose state, k_l, is questionable. This is because the ambient water flows into the pores of the sediment continuously, rather than solely when the porosity is maximum, n_l, although it was shown by Van Rhee (2015) that the factor $(1-n_0)k_l/\delta n$ can be approximated using $10k_0$, where k_0 is the *in situ* hydraulic conductivity. Additionally, Eq. (1) is emphatically invalid when the breach face is steeper than 90° the like of which was observed at the toe of the breach face in the experiments of Alhaddad et al. (2020c).

Towards a step forward in predicting the erosion velocity of the breach face, Eq. (1) was extended, using sediment pick-up functions, to more realistic formulas by Mastbergen and Van den Berg (2003) and Van Rhee (2015). These two formulas account for the contribution of turbidity currents to sediment erosion. Mastbergen and Van den Berg (2003) adopted the sediment pick-up function of Winterwerp et al. (1992) and developed the following equation:

$$v_e = u_s\left(\frac{v_w}{2u_s} + \sqrt{\left(\frac{v_w}{2u_s}\right)^2 + \frac{\phi_p \Delta k_l}{u_s \delta n}}\right), \tag{2}$$

where v_e is the net erosion velocity perpendicular to the breach face, $u_s = \sqrt{\Delta g d_{50}}$ is Shields velocity for sand grains, in which d_{50} is the median sediment grain size, and ϕ_p is an empirical non-dimensional pick-up function. On the other hand, Van Rhee (2015) adopted the sediment pick-up function of Van Rhee and Talmon (2010) and a modified critical Shields parameter taking into account the effect of dilatancy and a sloping bed, resulting in the following relationship:

$$v_e = \frac{0.000616\sqrt{g\Delta d_{50}}\;\frac{\theta}{\theta'_{cr}}\;\frac{1-n_0-c_b}{1-n_0} - w_s c_b \cos\alpha}{1-n_0-c_b}, \tag{3}$$

where c_b is the near-bed concentration, w_s is the particle settling velocity, θ is Shields parameter, and θ'_{cr} is a modified critical Shields parameter (see Section 4.2).

The predictive ability of Eqs. (2) and (3) was explored by Alhaddad et al. (2021) using momentary experimental data from a period during which surficial slides did not occur. It was found that Eq. (2) provides good agreement with the data, while Eq. (3) tends to overestimate the erosion velocity, with larger overestimations for steeper breach faces.

3.2. Assessment method of breaching mode

The evaluation of whether the failure during breaching will gradually grow in size (destabilizing breaching) or diminish (stabilizing breaching) is crucial for ensuring the safety of underwater infrastructure in the vicinity as well as flood defence structures. In previous studies of breaching (Van Rhee, 2015; Van Rhee, 2019), an empirical assessment method has been developed. This method is based on a simple geometric argument, considering the difference between the slope angles at the toe and top of the breach face and involving an existing empirical relation for the steady slope angle that eventually develops for a given sediment flux. Recently, Alhaddad et al. (2023), through experimental measurements, investigated the validity of this assessment method and found a mean absolute percentage error (MAPE) of 92% in the prediction of the slope height change.

To adequately evaluate the breaching mode, a more fundamental 3D approach is necessary. This approach should be capable of capturing the dynamics of the breach face, turbidity currents generated during breaching, the occurrence of surficial slides, and the sedimentation processes occurring down the base of the breach face.

4. Numerical models of breaching-generated turbidity currents

Breaching-generated turbidity currents largely control the evolution of the breaching failure and the fate of eroded sediment. Most importantly, there is a two-way coupled interaction between the breaching-generated turbidity currents and the breach face. Therefore, a number of numerical studies were conducted to investigate breaching-generated turbidity currents. In these studies, the interaction between the bed and the turbidity current is taken into account by using bed boundary conditions (i.e., a wall function for the momentum conservation and a pick-up function for the conservation of sediment mass). In this section, we provide an overview of these numerical studies, highlighting both their strengths and weaknesses.

4.1. Layer-averaged model

The evolution of turbidity currents can be described by integrating the conservation equations for momentum, fluid mass, and sediment mass over the depth of the current, including sediment erosion at the bed and water entrainment at the upper boundary of the current as source terms. Using the layer thickness h [m], the layer-averaged velocity in the stream-wise direction U [m/s], and the layer-averaged volumetric suspended sediment concentration C [-] as independent variables, and assuming a steady state, these equations read as follows,

$$\frac{\mathrm{d}(U^2h)}{\mathrm{d}s} = -\frac{1}{2}\,\Delta g\frac{\mathrm{d}(Ch^2)}{\mathrm{d}s} + \Delta g Ch\,\sin\alpha - u_*^2, \tag{4}$$

$$\frac{\mathrm{d}(Uh)}{\mathrm{d}s} = e_w U, \tag{5}$$

$$\frac{\mathrm{d}(UCh)}{\mathrm{d}s} = v_e(1-n_0), \tag{6}$$

where s [m] is the stream-wise coordinate along the breach face, Δ [-] is the relative submerged density of sediment, g [m/s^2] is the gravitational acceleration, α [-] is the slope angle of the breach face, e_w [-] is the water entrainment coefficient, and v_e [m/s] is the net erosion velocity perpendicular to the breach face. Three relationships can be found in the literature to predict v_e (i.e, Mastbergen and Van den Berg (2003), Van Rhee (2015), Alhaddad et al. (2020a)), which account for the sediment dilative behavior and the sloping bed. The bed shear velocity u_* [m/s] is calculated using the relation $u_*^2 = C_f U^2$, in which C_f [-] is a dimensionless bed friction coefficient.

Utilizing such a model, Mastbergen and Van den Berg (2003) simulated a flushing event in Scripps Submarine Canyon, demonstrating the ability of breaching-generated turbidity currents to excavate a submarine canyon. Similarly, Eke et al. (2011) simulated a flushing event in Monterey submarine canyon. Alhaddad et al. (2020b) also applied this model to breaching, illustrating that the results are highly sensitive to the sediment erosion closure term, v_e.

Since the model described above renders results quickly, it can be valuable for a first order study. Additionally, this model can be coupled

with the Exner equation for bed sediment conservation to capture the temporal evolution of the breach face. Nonetheless, the occurrence of the surficial slides and their effect on the turbidity currents (they feed material to the turbidity current, increasing its erosive capacity) cannot be captured by this model. Besides, owing to the feedback between the suspended sediments and flow turbulence, the dynamics of turbidity currents are highly complicated. Consequently, modeling turbidity currents by layer-averaged equations is a greatly simplified approach (Kneller and Buckee, 2000), requiring several empirical closure relations, such as the near-bed concentration, water entrainment at the upper boundary and bed friction coefficient. These empirical relations reduce the accuracy of the simulation results.

4.2. 2DV numerical model

A two-dimensional vertical (2DV) drift-flux model, originally developed for the sedimentation process in a Trailing Suction Hopper Dredge (Van Rhee, 2002), was extended to simulate the breaching process by Van Rhee (2015). The horizontal and vertical momentum equations applied on a control volume $d\Omega$ with a surface area dA read, respectively,

$$\frac{\partial}{\partial t}\int_{\Omega}\rho_m u \; d\Omega + \int_A \rho_m u\boldsymbol{u}\cdot\boldsymbol{n} \; dA = \int_A (\boldsymbol{\tau}\cdot\boldsymbol{n})_x \; dA - \int_A p n_x \; dA \tag{7}$$

$$\frac{\partial}{\partial t}\int_{\Omega}\rho_m w \; d\Omega + \int_A \rho_m w\boldsymbol{u}\cdot\boldsymbol{n} \; dA = \int_A (\boldsymbol{\tau}\cdot\boldsymbol{n})_z \; dA - \int_A p n_z \; dA - \int_{\Omega}\rho_m g \; d\Omega \tag{8}$$

where $\boldsymbol{u}$ is the mixture flow velocity with horizontal component u and vertical component w, p is pressure, ρ_m is the density of the sediment-water mixture, $\boldsymbol{\tau}$ is shear stress, $\boldsymbol{n}$ is the normal vector pointing outward of the control volume with horizontal component n_x and vertical component n_z. The continuity equation for incompressible flows in conservative notation reads:

$$\int_A \boldsymbol{u}.\boldsymbol{n} \; dA = 0. \tag{9}$$

The particle size distribution is approximated with a finite number N of different particle diameter ranges. The concentration of a certain fraction is c_k and D_k is the midpoint of the corresponding particle diameter range. The mixture density ρ_m is computed using the concentration of the different fractions:

$$\rho_m = \overline{c}\rho_s + \left(1-\overline{c}\right)\rho_w, \tag{10}$$

where ρ_w is water density and ρ_s is density of sediment particles and $\overline{c}$ is the total volumetric concentration given by:

$$\overline{c} = \sum_{k=1}^{N} c_k. \tag{11}$$

The transport equation for a certain fraction j in conservative form reads:

$$\frac{\partial}{\partial t}\int_{\Omega} c_j \; d\Omega + \int_A c_j \vec{v_{z,j}}.\vec{n} \; dA = \int_A \left(\Gamma\nabla c_j\right).\vec{n} \; dA, \tag{12}$$

where ∇ denotes the spatial gradient operator and $\vec{v_{z,j}}$ is the velocity vector of the sediment particle size j. The first term gives the rate of change of the concentration of a fraction, while the second term represents the transport of that fraction due to advection. In the right-hand side, the diffusive transport (caused by turbulence) is given. The diffusion coefficient Γ is related to the eddy viscosity ν_e with the Schmidt-Prandtl number σ:

$$\Gamma = \frac{\nu_e}{\sigma}. \tag{13}$$

Generally, this number is regarded as constant throughout the computational domain Rodi (1993). Uittenboogaard (1995) showed that in free turbulence, even in highly stratified conditions, $\sigma = 0.6$ can be used. The mixture model approach is used, implying that in the horizontal direction the particle velocity is equal to the mixture velocity as computed with the RANS equations. In the vertical direction, a slip velocity between the fluid velocity and grain velocity is assumed due to gravity (settling of the particles). For a mono-sized mixture (only one particle diameter present), the slip velocity equals the settling velocity of that size, which is a function of the concentration:

$$w_s = w_0\left(1-c\right)^a, \tag{14}$$

where a is the exponent of hindered settling function.

For a multi-sized mixture, it is more complicated. The different sizes have a mutual influence. It is shown in Mirza and Richardson (1979) and Van Rhee (2001) that the vertical velocity of a particle of size D_j in a mixture of N different particle sizes reads:

$$v_{z,j} = w + \sum_{k=1}^{N} c_k v_{s,k} - v_{s,j}, \tag{15}$$

where the slip velocity $v_{s,j}$ reads:

$$v_{s,j} = w_{0,j}\left(1-\overline{c}\right)^{a_j-1}, \tag{16}$$

in which $w_{0,j}$ is the settling velocity of a single particle with diameter D_j and a_j is the hindered settling exponent of that particle size. The value of this exponent varies between 2.6–5, depending on the particles size (Richardson and Zaki, 1954; Rowe, 1987). Turbulence closure is obtained with the k - ϵ turbulence model with a buoyancy term to include the effect of density stratification on turbulence damping. At the bed boundary, a sedimentation-erosion condition is applied. The sedimentation velocity v_{sed}, defined as the vertical velocity of the seabed (interface between settled sediment and water/mixture above the bed, positive when sedimentation takes place) reads:

$$v_{sed} = -v_e = \frac{S-E}{\rho_s\left(1-n_0-c_b\right)} \tag{17}$$

where S is sedimentation flux, E is erosion/pick-up flux, n_0 is the porosity of the settled sediment and c_b is near-bed concentration. The pick-up flux is computed taking into account the effect of dilatancy using a modified critical Shields parameter as described in Van Rhee (2010, 2015). The critical Shields parameter including the effect of dilatancy and a sloping bed reads (Van Rhee, 2010):

$$\theta'_{cr} = \theta_{cr}\left(\frac{\sin(\phi-\alpha)}{\sin\phi} + v_e\frac{\delta n}{k_l(1-n_0)\Delta}\right) = \theta_{cr}(R_\alpha + A_1 v_e) \tag{18}$$

where R_α and A_1 represent the effect of slope and dilatancy on the critical Shields parameter, respectively. This modified critical Shields parameter has the advantage that it yields the erosion velocity for slopes with angles larger than the internal friction angle (Van Rhee, 2010).

A cut-cell technique (Yang et al., 1999) is used to track the position of the bed in the grid cells and the bed position is updated every time step. The porosity n_0 of the settled bed is an input value in the model, although a more accurate representation would involve retrieving this value based on the particle size distribution or the bed shear stress during sedimentation; a correlation between the latter and n_0 was shown in Van Rhee (2002). The model was validated against the experiments of Weij (2020) in Van Rhee (2019) for the temporal evolution of the breach face. The agreement between the experiments and the numerical model was good for the finer sand (120 micron). However, for the coarser sand (332 micron), the regression velocity of the slope was overestimated by the model.

A shortcoming of the use of Eq. (17) is that the reference height for the near-bed concentration c_b is unclear. Commonly, the value of c_b is retrieved from the first cell above the bed, resulting in c_b being highly sensitive to the resolution of the mesh above the bed. Towards tackling this problem, a dynamically consistent definition of the reference height for c_b was recently proposed by Keetels et al.

(2023). Another limitation of this model is that the occurrence of the surficial slides is not included. Furthermore, the model described above is two-dimensional, while the breaching process is essentially three-dimensional, as discussed earlier. Additionally, the model is based on suspended sediment transport and is therefore unsuitable for situations where bed-load transport becomes the dominant mechanism. Nevertheless, the model is useful for large-scale practical problems, such as (2D) breaching, hopper sedimentation in dredging vessels and back-filling of submarine pipe trenches (Van Rhee, 2011).

4.3. Large eddy simulations (LES)

The utilization of large eddy simulations offers the notable advantage of resolving the larger turbulent scales, which contain the majority of the turbulent kinetic energy. This feature enables the accurate representation of the effect of density gradients on turbulence production, while also incorporating the anisotropic nature of turbulence. Thus, large eddy simulations provide an abundance of valuable insights into the physical behavior and structure of turbidity currents and particularly into the turbulence structure. To this end, Alhaddad et al. (2020a) presented 3D large-eddy-resolving numerical simulations, delivering deeper insights into the flow structure and hydrodynamics of breaching-generated turbidity currents. A brief description of the used model is presented below.

Following the mixture approach, the concentrations of the individual sediment fractions are solved independently, whereas a set of momentum equations is solved for the water-sediment mixture. Each sediment fraction has its own drift velocity, $\boldsymbol{u}_d$, described as the velocity of the sediment relative to the water-sediment mixture, which involves a correction of the mixture velocity with the sediment settling velocity.

The balance equations for the total mass and momentum of the mixture read, respectively,

$$\frac{\partial \rho_m}{\partial t} + \nabla \cdot (\rho_m \boldsymbol{u}) = 0, \tag{19}$$

$$\frac{\partial \rho_m \boldsymbol{u}}{\partial t} + \nabla \cdot (\rho_m \boldsymbol{u} \otimes \boldsymbol{u}) = -\nabla P + \nabla \cdot \boldsymbol{\tau} + (\rho_m - \rho_w)\boldsymbol{g}, \tag{20}$$

where t denotes time and P is the excess pressure over the hydrostatic pressure. It should be noted that the slip-stress is ignored in Eq. (20). A discussion on this assumption will follow in Section 5.2.

The transport equation reads,

$$\frac{\partial c}{\partial t} + \nabla \cdot (\boldsymbol{u}_s c) = \nabla \cdot (\Gamma \nabla c), \tag{21}$$

in which $\boldsymbol{u}_s = \boldsymbol{u} + \boldsymbol{u}_d$ is the velocity of the sediment fraction, and Γ is the diffusivity.

For a well-posed problem, Eqs. (19), (20) and (21) must be accompanied by appropriate boundary conditions. Moreover, the interaction of the turbidity currents with the breach face involves the bed shear stress $\boldsymbol{\tau}_b$, and the sedimentation flux S and erosion flux E. An empirical pick-up function is required to calculate the latter.

It is worth noting that the model above can be coupled with bed equations to capture the temporal evolution of the breach face. However, LES is computationally demanding, since it requires resolving a large range of turbulent eddy scales, which can span several orders of magnitude. This means that the simulation must be performed at a very high spatial resolution to capture the details of the large eddies. Additionally, the time step for the simulation must be small enough to accurately capture the dynamics of the turbulent eddies.

A shortcoming of the model presented above is that it underestimates the thickness of the current and in particular the thickness of the inner region, as reported in Alhaddad et al. (2020a). This underestimation may partly relate to a missing feedback from the sediment particles to the flow, leading to less momentum exchange and mixing. The thickness underestimation could also be attributed to the missing interaction between sediment particles. In the inner region of breaching-generated turbidity currents, as revealed by Alhaddad et al. (2020c), the particle concentration is typically much higher than the Bagnold limit (Bagnold, 1962), where particle–particle interactions play a role in supporting the particles; energy exchanged by particle collisions aid in keeping them suspended (Mulder and Alexander, 2001). Another limitation of this model, similar to layer-averaged and 2DV models, is that it does not account for the occurrence of surficial slides and thus the ensuing increase of the erosive capacity of the turbidity current.

5. Numerical models of breaching interface

A complete numerical model for breaching should involve the following processes: soil dilatancy, pore-pressure feedback, soil hardening, inflow of ambient water into pores, large shear deformation of the soil, pick-up of sediment from the sediment-water interface, formation of a turbidity current, settling of particles and build up of new slope down the toe of the breach face.

Lagrangian–Eulerian approaches are commonly employed to model a complete fluid–particle - particle–particle coupling. A noteworthy example is the Discrete Element Method (DEM) - Computational Fluid Dynamics (CFD) coupling. The DEM handles the discrete particulate phase while the CFD models the continuous fluid phase. Xu et al. (2019) and Ikari and Gotoh (2023) have successfully studied granular column collapses both in terms of runout distance and deposition shape. However, the high computational cost associated with these simulations restricts the application to small scales where some of the breaching features such as turbidity currents or surficial slides are not fully captured. Despite this limitation, DEM-CFD studies, like the recent work by Lu et al. (2023) exploring turbidity currents of low concentrations ($C = 0.01$) over a simplified bed topography, can shed light on the complex physics of turbidity currents. Another hybrid Lagrangian–Eulerian approach worth mentioning is the Material Point Method (MPM), which is particularly well-suited for simulating large deformation problems involving granular materials. Li et al. (2023) demonstrated MPM's effectiveness in predicting flow slides and turbidity currents. Nonetheless, Ceccato et al. (2018) and Zhao and Liang (2018) pointed out that MPM results are very sensitive to the choice of constitutive relations used to describe the material behavior. Although inaccurate constitutive closures may compromise the results, MPM remains a promising tool for engineering applications.

In contrast to Lagrangian–Eulerian approaches, two-phase flow formulations have been recently employed to model the breaching phenomenon. Within the two-phase framework, there are two main strategies. The first strategy is to solve the momentum balance for the particle phase and the fluid phase separately. This method is known as the Euler–Euler approach. The second approach is to solve one equation for the sum of the momentum balances of both phases and a separate equation for the relative velocity between the phases. This approach is called the mixture approach and was introduced in Section 4. The differences in the formulation result from the closure, which will be discussed in this section.

5.1. Euler-Euler approach

An Euler–Euler (E–E) model is a potential candidate for simulating the slope failure and the resultant turbidity current because it models the particle–particle interactions, the fluid–particle interactions, and the fluid turbulence. The governing equations of the water and sand are obtained by performing averaging processes, (see, e.g., Hsu et al., 2003). The continuity equations for water and sand are given by

$$\frac{\partial [\rho_w (1-c)]}{\partial t} + \nabla \cdot [\rho_w (1-c)\boldsymbol{u}_w] = 0, \tag{22}$$

and

$$\frac{\partial (\rho_s c)}{\partial t} + \nabla \cdot (\rho_s c \boldsymbol{u}_s) = 0, \tag{23}$$

where the subscript s/w represents the sediment/water, respectively. Fig. 11b illustrates the cell averaged concentrations in a 2D grid where

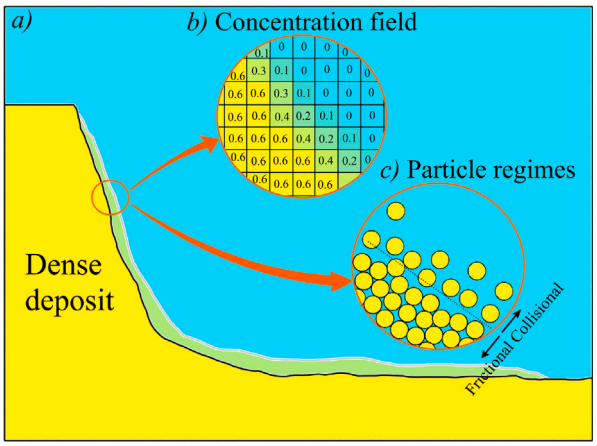

Fig. 11. (a) Scheme of the breaching process, b) discretization of the concentration (c) field near the interface and c) different particle regimes found during a granular flow.

a diffusive interface is represented by concentrations cells that range from $c = 0$ to $c = 0.6$. The momentum equations for water and sand can be written in the following conservative form:

$$\begin{aligned}\frac{\partial \rho_w (1-c)\boldsymbol{u}_w}{\partial t} &+ \nabla \cdot [\rho_w (1-c)\boldsymbol{u}_w \otimes \boldsymbol{u}_w] \\ &= \rho_w (1-c)\boldsymbol{g} - (1-c)\nabla p_w \\ &+ \nabla \cdot \boldsymbol{\tau}_w + \boldsymbol{f}_{in},\end{aligned} \tag{24}$$

and

$$\begin{aligned}\frac{\partial \rho_s c \boldsymbol{u}_s}{\partial t} &+ \nabla \cdot (\rho_s c \boldsymbol{u}_s \otimes \boldsymbol{u}_s) = \rho_s c \boldsymbol{g} - c\nabla p_w \\ &- \nabla p_s + \nabla \cdot \boldsymbol{\tau}_s - \boldsymbol{f}_{in},\end{aligned} \tag{25}$$

where p_w is the fluid pressure, p_s stands for the particle pressure, $\boldsymbol{\tau}_w$ and $\boldsymbol{\tau}_s$ denote the fluid and particle shear stresses and $\boldsymbol{f}_{in}$ accounts for the coupling between the fluid and sediment phase through the drag force:

$$\boldsymbol{f}_{in} = c(1-c)K(\boldsymbol{u}_s - \boldsymbol{u}_w + \boldsymbol{u}_{dr}), \tag{26}$$

where K is the drag parameter and $\boldsymbol{u}_{dr}$ is the turbulent drift velocity, which represents turbulent suspension effects (Keetels et al., 2018; Chauchat and Guillou, 2008).

The key to E–E modeling lies in selecting proper closure models for $\boldsymbol{\tau}_w$, $\boldsymbol{\tau}_s$, p_s, and $\boldsymbol{f}_{in}$ according to the physics behind the problems to be solved. In this context, we refer the reader to Chauchat et al. (2017) and Lee et al. (2022) whose work include several closure forms implemented in a two-phase flow framework.

In the framework of subaqueous dilative slope failure, special emphasis should be placed on dilatancy effects and pore pressure feedback to fully understand the physics behind the breaching process. Although Eq. (18) presented in Section 4.2 leads to an erosion velocity that takes into account a certain degree of porosity changes at the breach face, the model is insufficient to correctly capture the grain rearrangements and local changes in permeability as the soil expands. Dilatancy effects and pore pressure feedback are a crucial part of the breaching process with evident consequences on the mobility of the granular material. Thus, in the E–E framework, several approaches (Lee, 2021; Montellà et al., 2021) have been proposed to model this important coupling. The details of the closures slightly differ, however, in both models the dilatancy is embedded in the particle pressure, which can be decomposed as the sum of two terms:

$$p_s = p_{sd} + p_{ss}, \tag{27}$$

where p_{sd} results from dynamic effects and depends on the strain rate (collisional regime), and p_{ss} results from the enduring contacts between particles (frictional regime). Both regimes are illustrated in Fig. 11c. Early E–E models used $p_{ss} - c$ relationships as closure forms for p_{ss} (Lee et al., 2016; Chauchat et al., 2017):

$$p_{ss} = \begin{cases} 0 & c < c_{pl} \\ E_m \dfrac{(c - c_{pl})^3}{(c_{rcp} - c)^5} & c \geq c_{pl}, \end{cases} \tag{28}$$

where E_m is an elastic modulus, c_{rcp} is the random close packing and c_{pl} is the reference solid volume fraction. This expression is rate independent and although this type of relationship can reproduce the breaching process, the soil expansion is too rapid due to the purely elastic behavior of the model, resulting in unreasonable pore pressures (Lee and Huang, 2018). Recently, Lee (2021) proposed an evolution equation to determine p_{ss}, which is able to capture the relaxation process of p_{ss} under shearing conditions and correctly predict the shear-induced dilation. With such approach, Lee (2021), Lee and Chen (2022) reproduced the small scale breaching experiments of Rondon et al. (2011) and Lee and Chen (2022). However, the approach of Lee (2021) has not been applied to large scale breaching experiment.

Similarly, Montellà et al. (2021) adjusted Eq. (28) to include the plastic effects that arise from local rearrangements during plastic shearing deformations through changes in c_{pl} (c_{pl} in Eq. (28) is considered a variable instead of a constant). The evolution of c_{pl} is governed by an equation derived from a plastic flow rule and Montellà et al. (2023) proved that this approach is suited to reproduce the dynamics of the breach face. Phan et al. (2022) used a similar approach and successfully modeled the breaching experiment of Rondon et al. (2011). In addition to the plastic effects embedded as changes in the contact pressure (p_{ss}), dilatancy effects due to shearing deformations are also manifested in the dynamic solid pressure (p_{sd} in Eq. (27)). Indeed, E–E approaches frequently opt to model the particle shear stress ($\boldsymbol{\tau}_s$) using the $\mu(I)$-rheology, which assumes the ratio of particle shear stress and the particle pressure is a state-dependent friction coefficient ($\mu(I)$). Several formulas for the shear-rate dimensionless number I are found in the literature depending on the flow regime (Da Cruz et al., 2005; Jop et al., 2006; Boyer et al., 2011; Trulsson et al., 2012). From the definition of the dimensionless number I, one can derive an expression for the dynamic shear-rate dependant pressure (p_{sd}) that results from the overall expansion of the soil under shear deformations.

Regarding the turbidity current, where the turbulence dominates, the key closures are $\boldsymbol{\tau}_w$ and $\boldsymbol{u}_{dr}$. Lee (2019) adopted two-equation turbulence model ($k-\epsilon$) and reproduced well the measured front velocity of the dilute lock-release turbidity current (Gladstone et al., 1998). However, the flow structure and the concentration distribution inside the turbidity current was not examined carefully. The key challenge in the breaching process is to accurately simulate the pickup process occurring at the breach face, which is the source of sediment for the turbidity current. This pickup process takes place at a very small scale, typically at the length scale of the particles and therefore requires either a very fine resolution or an accurate parametrization. This is still an open question for Euler–Euler models.

The primary weakness of the E–E modeling is definitely its high computational cost. As mentioned above, in order to capture the sharp variation of physical properties near the sediment bed, the size of the numerical cells should be of the order of the sand particles. This is affordable for a small-scale experimental configuration such as Rondon et al. (2011) but too expensive for 'large-scale' experiments such as those presented by Alhaddad et al. (2020c, 2023). Additionally, p_s is highly sensitive to c in the limit of large c, hence, a small time step is required for numerical stability. Aforementioned limitations suggest that, at this moment, E–E modeling is suitable for exploring the physics rather than practical applications.

5.2. Mixture approach

The equations for the mixture, which are already presented by Eqs. (19) and (20), can be derived from the more fundamental E–E model by summing Eqs. (22) and (23) and Eqs. (24) and (25), respectively. Recombining the convection terms also yields an additional slip-stress term (see e.g., Savage et al. (2014), Weij (2020)), which is missing in Eq. (20). For low Stokes number flows, the contribution of this term is negligible. This assumption is typically satisfied for large scale applications with fine sediments. For high speed flows and larger particles, the slip-stress contribution should be incorporated. It is also expected that the Stokes number increases when moving closer towards the sand bed. Therefore, the slip-stress contribution needs to be incorporated in mixture models that aim to resolve near-bed sediment transport.

The advantage of the mixture approach with respect to the E–E approach is that the interfacial coupling term, given in Eq. (26), cancels in this summation. In general, this favors numerical stability in strongly coupled dispersed multiphase systems. On the other hand, the uncertainty in the modeling is transferred to the modeling of the relative velocity between the particles and the mixture and the diffusivity coefficient in Eq. (21). In the low Stokes number regime, the relative velocity can be approximated with the terminal settling velocity of particles in stagnant water. This strongly simplifies the modeling and makes this approach particularly powerful for modeling sediment plumes in environmental applications and sedimentation processes in hopper dredgers.

Based on these experiences, Weij (2020) explored this approach to model the breaching process. The pore-pressure feedback mechanism was incorporated in a different way than in the E–E models discussed above. Instead of introducing a dynamic pressure p_{sd} and static pressure p_{ss} (see Eq. (27)), Weij (2020) directly imposed the expected shear-induced rate of change of the solid concentration. This estimate was based on the deviation of the concentration from the equilibrium concentration described by the $\mu(I_v)$ rheology and the instantaneous shear rate. A basic volume balance and Darcy's law then result in a Poisson equation for the excess pore pressure, where the shear-induced rate of change of the solid concentration serves as a source term on the right-hand side of this equation. The effective stress, required for the feedback to the soil strength model, was then computed by combining the computed excess pore pressure and the mixture pressure P. The mixture pressure is governed by a separate Poisson equation that follows from the momentum balance, Eq. (20), in conjunction with the mass balance, Eq. (19). This is almost identical to a single phase flow, with the exception that the right-hand side of the Poisson equation for P contains the time derivative of the mixture density as an explicit source term. Finally, the feedback to soil strength was incorporated via a modified viscosity of the mixture in accordance with the effective stress, again using the $\mu(I_v)$ rheology. Since the same rheological ingredients are applied as in the E–E approach, though at a different location in the model, we do not expect substantial differences regarding the build up of a negative excess pore pressure by shear in dense soil, dissipation of this pressure, the loss of soil strength and thus the basic breaching process.

The most significant difference with respect to the more fundamental E–E models is that this approach allows for an additional closure of the diffusivity coefficient Γ. For computational cells at the sand bed interface, identified by a fixed reference concentration, this value was chosen such that the diffusive flux $\Gamma\partial_x C$ is consistent with the existing empirical pick-up relations. Likewise, traditional rough wall functions were applied to describe the momentum transfer from the suspension region to the bed region. The additions of the wall-functions and pick-up relations to the mixture model could potentially represent the effect of the turbidity current on the enhancement of the breaching process as identified by Alhaddad et al. (2020c) and the sedimentation process down the toe of the breach face.

Table 1
Limitations and applications of the analytical and numerical approaches employed to model the breaching process.

Approach	Limitations	Application/advantages
Wall velocity expression	(a) Turbidity currents and surficial slides are not modeled (b) 3D effects and bed-load transport are neglected	(a) First order approach to model the erosion velocity of the breach face
Layer-averaged model	(a) Surficial slides are not modeled (b) Turbidity currents are simplified (c) 3D effects and bed-load transport are neglected (d) No particle–particle and particle–fluid interactions	(a) Renders results quickly (b) Suitable for first order studies (c) Can be coupled with the Exner equation
2DV RANS mixture model	(a) Surficial slides are not modeled (b) 3D effects and bed-load transport are neglected (c) Low Stokes number approximation of particle–fluid interaction	(a) Useful for large-scale practical problems, such as 2D breaching, hopper sedimentation in dredging vessels and back-filling of submarine pipe trenches
LES mixture model	(a) Surficial slides are not modeled (b) Bed-load transport is neglected (c) Low Stokes number approximation of particle–fluid interaction (d) Computationally demanding	(a) Accurate representation of the effect of density gradients on turbulence production (b) Detailed structure and hydrodynamics of breaching-generated turbidity currents
Coupled fluid–soil approach (mixture model)	(a) High computational cost (b) Needs closure terms for sediment erosion velocity	(a) Suitable to study the physical mechanisms at the micro and meso scales
Coupled fluid–soil approach (E–E model)	(a) High computational cost	(a) Suitable to study the physical mechanisms at the micro and meso scales (b) Does not need closure terms for sediment erosion velocity (c) Suitable to investigate both breaching and liquefaction.

Several comparisons with experiments were performed by Weij (2020). The migration velocity of the breach face was well retrieved. It was found, however, that the model substantially overestimates the erosion rate at the slope down the toe of the breach face, resulting in lower slope angles compared to the experiments. The reason of this mismatch was unclear. A condition that could have played a role is that the sand-flux in the experiments was relatively low. A separate set of computations with a given sediment flux also indicated that the slope angle, at low sediment flux, was significantly lower compared to the experiments of Mastbergen et al. (1988). The formation of the slope angle down the toe is very important to determine the temporal evolution of the breach height, see Alhaddad et al. (2023). The second limitation of the model of Weij (2020) was the usage of fixed reference concentration to identify the bed. This does not allow the formation of a looser bed down the toe, which could result in pore water over pressure situations and trigger a liquefaction event in reality. The model of Montellà et al. (2021) could potentially carry this physics by considering a variable reference concentration c_{pl} in Eq. (28).

Albeit these shortcomings, the mixture approach of Weij (2020) or even simpler formulations such as Savage et al. (2014) could bridge the gap between the fundamental E–E models and the models designed for large scale applications described in Section 4, which only mimic the presence of a breach face by adjusting the boundary conditions.

A brief summary of the limitations and applications of analytical and numerical approaches discussed above is presented in Table 1.

Table 2
Properties of sands used in the experiments of Alhaddad et al. (2023).

	D_{50} (μm)	D_{15} (μm)	c_o	ϕ (°)
Exp. 8	120	80	0.585	35.8
Exp. 16	330	225	0.570	40.1

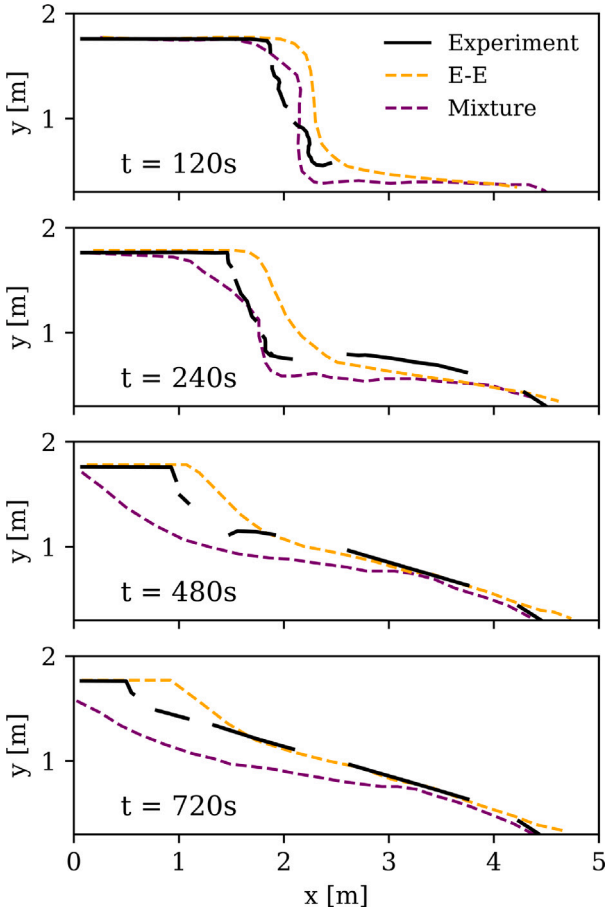

Fig. 12. Measured and numerical predictions of the deposit shape during Experiment 8.

6. Inter-comparison between numerical approaches

Two breaching experiments conducted by Alhaddad et al. (2023) (i.e., Experiment 8 and Experiment 16) were simulated using the aforementioned 2DV drift-flux, mixture and Euler–Euler approaches. These three approaches were selected for inter-comparison due to their capability to address the dynamic breach face. In the first two approaches, Eq. (18) was used to compute the modified critical Shields parameter and subsequently the local erosion velocity using the pick-up function of Van Rijn (1984). The median and 15th percentile grain size, initial volume fraction and internal friction angle of the two experiments are summarized in Table 2.

Fig. 12 illustrates the temporal morphological changes in the sand deposit during the breaching process for Experiment 8. The steep breach face recedes slowly and moves horizontally by releasing particles. As the experiment progresses, the breach face diminishes in size and steepness. While both the mixture and Euler–Euler approaches generally capture the breaching behavior well, discrepancies arise when compared to the experimental data. Both models exhibit a rounding effect near the top of the breach face, an aspect not observed in the experiments. This rounding is more evident with larger grid cells and lower dilatancy factors (Weij, 2020; Montellà et al., 2023).

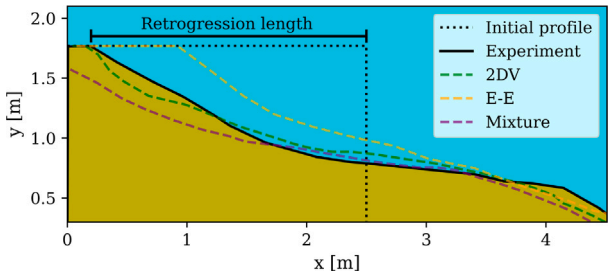

Fig. 13. Measured and numerical predictions of the final deposit shape for Experiment 8. The dotted line stands for the initial position of the granular column and the retrogression length indicates the wall evolution of a breaching event.

Table 3
Measured and predicted retrogression lengths (RL) for Experiments 8 and 16, and error (E) with respect to the experimental data.

	Exp.	2DV		Mixture		E–E	
	RL [m]	RL [m]	E [%]	RL [m]	E [%]	RL [m]	E [%]
Exp. 8	2.30	2.35	2.1	2.50	8.7	1.60	30.4
Exp. 16	1.31	2.12	61.8	1.79	36.6	1.10	16.0

Initially, the mixture model aligns with the experimental breach face position; however, after $t = 240$ s, it overestimates erosion velocities compared to experiments. In contrast, the E–E model shows a delayed start of breach face movement compared to experiments, but once in motion, it matches the velocity of the receding front observed in experiments. Concerning the final shape of the deposit, the E–E model successfully predicts a 20-degree slope deposit, closely resembling the experimental shape. Conversely, the mixture model simulation shows a slower buildup of slope at the breach face toe due to the higher erosion velocities.

The post-failure deposit shape can be visualized in Fig. 13. In addition to the numerical profiles obtained with the Eulerian approaches, the prediction of the 2DV drift-flux approach is also included in the comparison. Fig. 13 shows that the mixture model overpredicts the retrogression length, while the E–E approach underpredicts it. The 2DV drift-flux model, on the contrary, offers better results with a similar deposit shape and retrogression length to experimental data. Detailed quantitative results for retrogression lengths are summarized in Table 3, along with the corresponding errors relative to the experimental observations.

Fig. 14 displays excess pore pressure peaks shortly after lifting the gate in both experiments and Eulerian approaches. While the peak magnitudes are comparable, discrepancies arise in the evolution of pore pressure curves. Experiments indicate a significant pressure reduction right after the pressure peak, followed by a constant dissipation rate around $t = 25$ s. However, the E–E model exhibits a shifted pore pressure peak, potentially explaining the delay in breach movement observed in Fig. 12. Both models struggle to replicate the rapid pore pressure reduction post-peak, yet they manage to predict the dissipation rates observed in the experiments.

Regarding sensitivity to numerical parameters, both Weij (2020) and Montellà et al. (2023) highlight that lower dilatancy factor values result in higher erosion velocities. Similarly, the critical volume fraction significantly influences dilatancy, with lower values leading to lower erosion velocities due to accentuated dilatancy effects. Rounding at the breach face top heavily depends on grid size, with more rounding seen in larger grid cells and sharper corners in finer meshes. Larger grid cells also result in higher erosion velocities and quicker pore pressure dissipation.

In Experiment 16, with different sand characteristics, slightly different dynamics are manifested, showing an accelerated breaching due to the higher sand hydraulic conductivity. Fig. 15 illustrates the evolution

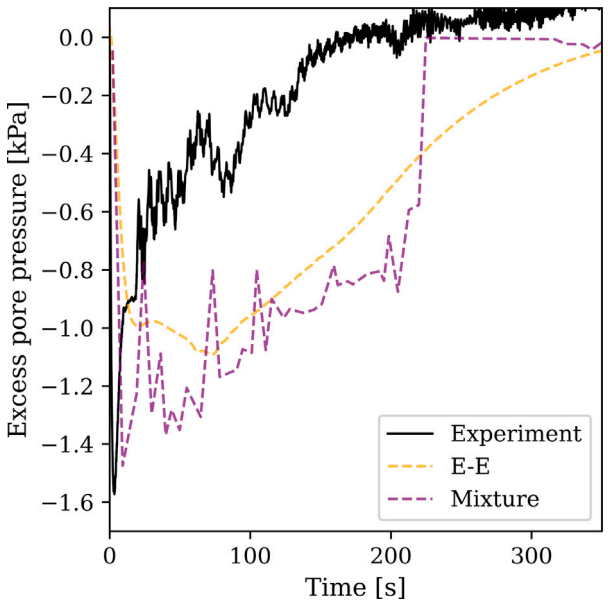

Fig. 14. Comparison of numerical and experimental excess pore pressures, collected at Point (x = 1.9 m, y = 1.0 m) for Experiment 8.

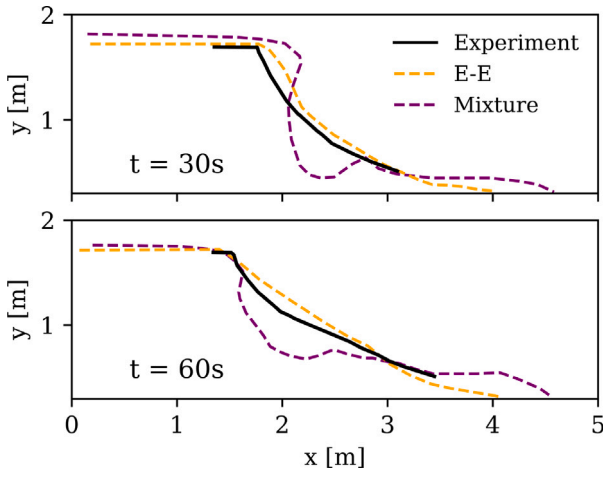

Fig. 15. Measured and numerical predictions of the deposit shape during Experiment 16.

of deposit morphology, well predicted by the E–E approach. In contrast to Experiment 8, where the 2DV drift-flux model was accurate in mimicking the final deposit shape, both Eulerian approaches offer better predictions of the morphological changes and the retrogression length in Experiment 16 (see Fig. 16). Table 3 reveals significant differences in the prediction of the retrogression length; the 2DV drift-flux model deviates from experimental observations by over 61.8%, whereas the mixture and E–E models deviate by 36.6% and 16.0%, respectively. Fig. 17 demonstrates the evolution of pore pressure in Experiment 16, showing good agreement between numerical and experimental data.

The investigation in this section shows that numerical models can satisfactorily predict the breaching process. They provide more information and better insights into the breaching mode and potential retrogression length compared to the simplified models outlined in Section 3. While both 2DV and Eulerian approaches (i.e., mixture and E–E models) exhibit fairly good performance in tracking morphological changes, it is worth mentioning that Eulerian approaches are better suited for examining the physical aspects of breaching. They offer access to local data (such as the pore water pressure) and insights

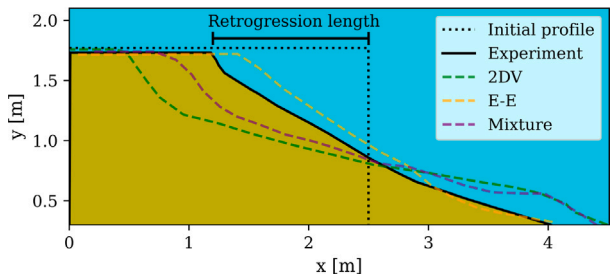

Fig. 16. Measured and numerical predictions of the final deposit shape for Experiment 16. The dotted line represents the initial position of the granular column, and the retrogression length indicates the wall evolution of a breaching event.

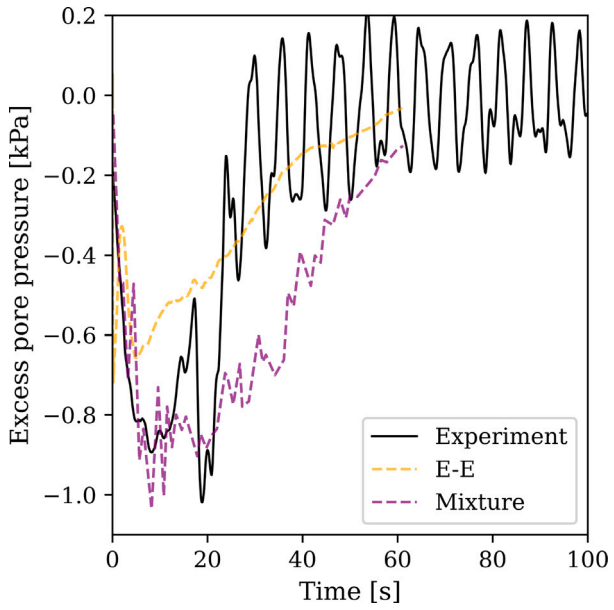

Fig. 17. Comparison of numerical and experimental excess pore pressures, collected at Point (x = 1.9 m, y = 1.0 m) for Experiment 16.

at a grain-scale level. Moreover, Eulerian approaches have demonstrated success in modeling shear slides, as evidenced in Montellà et al. (2023). Consequently, Eulerian models possess the capability to predict a wide range of failures, which is a crucial asset when dealing with heterogeneous soil.

7. Outlook and open questions

Through a systematic review and analysis of the current knowledge, laboratory and field observations and modeling approaches, this study has discussed the physical processes and numerical models pertaining to breaching. As a consequence, specific knowledge gaps, and limitations in the current models were identified. Here, we present potential future research directions to advance our understanding of the breaching phenomenon and improve modeling capabilities.

Addressing the above goals requires a multilevel approach, ranging from pore-pressure feedback mechanisms, release of particles and coherent sediment wedges from the breach face, generation of turbidity currents, and sediment erosion and deposition at the downstream region. In relation to pore-pressure feedback, the existing Euler–Euler approaches could be supplemented by alternative methods designed for hydro mechanical coupling in large-scale soil mechanical deformations, such as the MPM (Zheng et al., 2021) and the Particle Finite Element Method (Cremonesi et al., 2020). Moreover, DEM simulations arise as another potential to calibrate Euler–Euler models. DEM simulations

have successfully explored the dynamics of submerged granular collapses (Shademani et al., 2021) and they stand out for the ability to have access at the particle scale. Indeed, DEM-CFD approaches are valuable for gaining insights into the mobilization process of slides and obtaining a better understanding of particle stress and pore pressure distribution during soil failure. At the grain scale, DEM can provide relevant information that may influence the macroscopic behavior. For instance, Bao et al. (2023) studied the particle shape effects on submarine landslides. Furthermore, both MPM and DEM approaches have proven successful in modeling liquefaction (Scholtès et al., 2015; Ghasemi et al., 2018). These methods play a crucial role in filling knowledge gaps regarding hybrid flow slides (Van den Ham et al., 2022), where both liquefaction and breaching mechanisms are present. Additionally, more detailed experimental data on small soil samples are necessary to validate the dilatancy and soil hardening models or calibrate underlying parameters. This could involve traditional soil mechanical tests, such as the direct shear test, triaxial test and vane test, but also flow tests of sand layers, for example, on an inclined plane.

Various authors have studied the erosion capacity of turbidity currents (e.g., Garcia and Parker (1993)), but the influence of sediment bed state (i.e., loose or dense) remains an open question. Additionally, attention must be directed towards the bed-load transport rate, an important factor influencing the characteristics of the final deposit (Meiburg and Kneller, 2010). While the experimental study of Sequeiros et al. (2010) suggests the applicability of an existing formula derived for open channel flows (Meyer-Peter and Müller, 1948) to density currents, its suitability for turbidity currents requires additional scrutiny. Besides, existing bed-load transport formulas are primarily derived for near-flat bed conditions, implying that they need further improvement when applied to sloping beds, especially those exceeding the angle of repose. To address these research gaps, Euler–Euler flow simulations of turbidity currents running over an erodible bed need to be conducted using different turbulence modeling approaches, such as RANS and LES. These simulations should aim to determine the minimum grid criterion for a reasonable prediction of the pick-up flux or an accurate parametrization of this flux. Ideally, both aspects of these questions should be addressed to properly upscale turbidity currents in the context of breaching; prior experimental investigations (e.g., Alhaddad et al. (2020c)) showed that turbidity currents significantly increase the erosion rate at the breach face. Euler–Euler approach is computationally infeasible for engineering applications and large-scale experiments. Therefore, efforts should first focus on understanding the generation and development of turbidity currents on a small scale, which will enable the deviation of appropriate bed boundary conditions needed for computationally affordable models (as those presented in Section 4) and expand their applicability to practical scenarios. For instance, the distance of retrogression of a breaching event is the most critical practical result of such models for risk assessment, as it determines the extent of damage resulting from breaching.

The modeling aspect of breaching presents additional significant challenges waiting to be addressed. In particular, there is a pressing need to understand the triggering mechanisms of breaching, which is imperative for the development of appropriate initial and boundary conditions for modeling purposes. Here, the main difficulties lie in understanding the mechanisms that result in the submerged slope being steeper than the internal friction angle. While liquefaction and breaching are different mechanisms, similarities can be observed in the final morphology produced after the soil failure. Moreover, in some cases, dredging can contribute to liquefaction by altering the properties of the soil. Additionally, breaching can sometimes expose the freshly-deposited sediment on the downstream region to liquefaction, which can result in severe damage or collapse of buildings, bridges, or other infrastructure located nearby. On the other hand, liquefaction can enhance and even trigger breaching events as pointed out in Van den Ham et al. (2022). In this respect, Euler–Euler modeling is a potential tool to gain deeper insights into the transition between breaching and liquefaction. To better identify the triggering mechanisms in general, conducting field measurements and monitoring campaigns at locations where breaching has occurred previously would be highly beneficial.

Experimental investigations and field observations showed that the three-dimensionality plays an important role in the breaching process. Therefore, conducting three-dimensional experiments and numerical simulations will be instrumental to improving our understanding of the failure, including surficial slides, and turbidity current evolution across the breach face. This in turn will result in a better prediction of the morphological changes during a breaching event. Three-dimensional simulations require improved modeling capabilities. To this end, again, it would be advantageous to couple the simulation of turbidity currents to an advanced soil model that can adequately deal with spatial variations of soil characteristics, large deformations and pore-pressure feedback. This requires the integration of complementary research methodologies from the fields of fluid and soil mechanics.

CRediT authorship contribution statement

Said Alhaddad: Writing – review & editing, Methodology, Investigation, Formal analysis, Data curation, Conceptualization, Project administration, Supervision, Visualization, Writing – original draft. **Geert Keetels:** Writing – original draft, Project administration, Methodology, Investigation, Conceptualization. **Dick Mastbergen:** Visualization, Methodology, Data curation, Conceptualization, Writing – original draft. **Cees van Rhee:** Conceptualization, Methodology, Writing – original draft. **Cheng-Hsien Lee:** Conceptualization, Writing – original draft. **Eduard Puig Montellà:** Writing – original draft, Visualization, Methodology, Data curation, Conceptualization. **Julien Chauchat:** Methodology, Conceptualization.

Declaration of competing interest

The authors declare that they have no known competing financial interests or personal relationships that could have appeared to influence the work reported in this paper.

Data availability

Data will be made available on request.

Appendix A. Notation

A_1	Effect of dilatancy on the critical Shields parameter	-
a	Hindered settling exponent	-
C	Layer-averaged volumetric suspended sediment concentration	-
C_f	Dimensionless bed friction coefficient	-
c_b	Near-bed concentration	-
c_{pl}	Reference solid volume fraction	-
c_{rcp}	Random close packing	-
$\overline{c}$	Total volumetric concentration	-
D_j	The jth particle diameter	m
d_{50}	Median sediment grain size	m
E	Erosion/pick-up flux	kg/m^2 s
E_m	Elastic modulus	kg/m s^2
e_w	Water entrainment coefficient	-
$\boldsymbol{f}_{in}$	Coupling between the fluid and sediment phase through the drag force	kg/m^2 s^2
g	Gravitational acceleration	m/s^2
$\boldsymbol{g}$	Gravity vector	m/s^2

H	Breaching height	m
h	Layer thickness of turbidity current	m
K	Drag parameter	kg/m^3 s
k_l	Sediment hydraulic conductivity	m/s
n_0	In situ porosity of the sand	-
n_l	Maximum porosity of the sand	-
$\boldsymbol{n}$	Normal vector	m
P	Excess pressure over the hydrostatic pressure	kg/m s^2
p	Pressure	kg/m s^2
p_s	Particle pressure	kg/m s^2
$p_{sd/ss}$	p_s resulting from dynamic effects/ enduring contacts between particles	kg/m s^2
p_w	Fluid pressure	kg/m s^2
R_α	Effect of slope on the critical Shields parameter	-
S	Sedimentation flux	kg/m^2 s
s	The stream-wise coordinate along the breach face	m
t	Time	s
U	Layer-averaged velocity in the stream-wise direction	m/s
u	Horizontal flow velocity	m/s
$\boldsymbol{u}$	Mixture velocity vector	m/s
$\boldsymbol{u}_{dr}$	Turbulent drift velocity	m/s
u_s	Shields velocity for sand grains	m/s
$\boldsymbol{u}_{s/w}$	Velocity of the sediment/water fraction	m/s
u_*	Bed shear velocity	m/s
v_e	Net erosion velocity perpendicular to the breach face	m/s
v_{sed}	Sediment velocity	m/s
v_w	Wall velocity	m/s
w	Vertical flow velocity	m/s
w_0	Settling velocity	m/s
w_s	Particle settling velocity	m/s
α	Slope angle	^{o}
Γ	Diffusion coefficient	m^2/s
δn	$(n_l - n_0)/(1 - n_l)$	-
θ	Shields parameter	-
θ'_{cr}	Modified critical Shields parameter	-
ν_e	Eddy viscosity	m^2/s
$\rho_{s/w}$	Density of the sediment particles/ water	kg/m^3
ρ_m	Density of the sediment-water mixture	kg/m^3
τ	Shear stress	kg/ms^2
$\boldsymbol{\tau}$	Shear stress tensor	kg/ms^2
$\boldsymbol{\tau}_b$	Bed shear stress	kg/ms^2
$\boldsymbol{\tau}_{s/w}$	Particle/fluid shear stress	kg/ms^2
σ	Schmidt-Prandtl number	-
ϕ	Internal friction angle	^{o}
ϕ_p	Empirical pick-up function	-
Δ	Relative submerged density of sediment	-

References

ABS-CBN-News, 2013. What caused Candelaria, Zambales Beach collapse? ABS https://news.abs-cbn.com/nation/regions/06/25/13/what-caused-candelaria-zambales-beach-collapse.

Alhaddad, S., de Wit, L., Labeur, R.J., Uijttewaal, W., 2020a. Modeling of breaching-generated turbidity currents using large eddy simulation. J. Mar. Sci. Eng. 8 (9), 728.

Alhaddad, S., Elerian, M., 2024. Mitigating suspended-sediment environmental pressure in subsea engineering through colliding turbidity currents. Results Eng. 21, 101916.

Alhaddad, S., Labeur, R.J., Uijttewaal, W., 2019. The need for experimental studies on breaching flow slides. In: Proceedings of the Second International Conference on the Material Point Method for Modelling Soil-Water-Structure Interaction, No. 27. pp. 166–172.

Alhaddad, S., Labeur, R.J., Uijttewaal, W., 2020b. Breaching flow slides and the associated turbidity current. J. Mar. Sci. Eng. 8 (2), 67.

Alhaddad, S., Labeur, R.J., Uijttewaal, W., 2020c. Large-scale experiments on breaching flow slides and the associated turbidity current. J. Geophys. Res. Earth Surf. 125 (10), e2020JF005582.

Alhaddad, S., Labeur, R., Uijttewaal, W., 2021. Preliminary evaluation of existing breaching erosion models. In: 10th International Conference on Scour and Erosion. ISSMGE, pp. 619–627.

Alhaddad, S., Weij, D., van Rhee, C., Keetels, G., 2023. Stabilizing and destabilizing breaching flow slides. J. Mar. Sci. Eng. 11 (3), http://dx.doi.org/10.3390/jmse11030560.

Bagnold, R.A., 1962. Auto-suspension of transported sediment; turbidity currents. Proc. R. Soc. A 265 (1322), 315–319.

Bao, X., Wu, H., Xiong, H., Chen, X., 2023. Particle shape effects on submarine landslides via CFD-DEM. Ocean Eng. 284, 115140.

Beinssen, K., Neil, D.T., Mastbergen, D.R., 2014. Field observations of retrogressive breach failures at two tidal inlets in Queensland, Australia. Aust. Geomech. 49 (3), 55–64.

Boyer, F., Guazzelli, É., Pouliquen, O., 2011. Unifying suspension and granular rheology. Phys. Rev. Lett. 107 (18), 188301.

Breusers, H.N.C., 1977. Hydraulic excavation of sand. In: Proceedings International Course in Modern dredging.

Brilli, N., Stark, N., Nielsen, P., Callaghan, D., Manning, M., Culp, J., 2019. Field investigation of two retrogressive breach failures at amity point. In: Coastal Sediments 2019: Proceedings of the 9th International Conference. World Scientific, pp. 434–446.

Ceccato, F., Redaelli, I., di Prisco, C., Simonini, P., 2018. Impact forces of granular flows on rigid structures: comparison between discontinuous (DEM) and continuous (MPM) numerical approaches. Comput. Geotech. 103, 201–217.

Chauchat, J., Cheng, Z., Nagel, T., Bonamy, C., Hsu, T.-J., 2017. SedFoam-2.0: a 3-D two-phase flow numerical model for sediment transport. Geosci. Model Dev. 105194, 4367–4392.

Chauchat, J., Guillou, S., 2008. On turbulence closures for two-phase sediment-laden flow models. J. Geophys. Res.: Oceans 113 (C11).

Cremonesi, M., Franci, A., Idelsohn, S., Oñate, E., 2020. A state of the art review of the particle finite element method (PFEM). Arch. Comput. Methods Eng. 27, 1709–1735.

Da Cruz, F., Emam, S., Prochnow, M., Roux, J.-N., Chevoir, F., 2005. Rheophysics of dense granular materials: Discrete simulation of plane shear flows. Phys. Rev. E 72 (2), 021309.

De Bruin, M.P., Wilderom, M.H., 1961. Tussen Afsluitdammen en Deltadijken; Deel 1; Noord-Beveland, Middelburg.

Eke, E., Parker, G., Wang., R., 2009. Breaching as a mechanism for generating sustained turbidity currents. In: 33rd Internation Association of Hydraulic Engineering & Research Congress: Water Engineering for a Sustainable Environment. Vancouver, IAHR.

Eke, E., Viparelli, E., Parker, G., 2011. Field-scale numerical modeling of breaching as a mechanism for generating continuous turbidity currents. Geosphere 7 (5), 1063–1076.

Garcia, M., Parker, G., 1993. Experiments on the entrainment of sediment into suspension by a dense bottom current. J. Geophys. Res.: Oceans 98 (C3), 4793–4807.

Ghasemi, P., Martinelli, M., Cuomo, S., Calvello, M., 2018. MPM modelling of static liquefaction in reduced-scale slope. Numer. Methods Geotech. Eng. IX 2, 1041–1046.

Gladstone, C., Phillips, J.C., Sparks, R.S.J., 1998. Experimentation on bidisperse, constant-volume gravity curents: propagation and sediment deposition. Sedimentology 46, 833–843.

Hsu, T.-J., Jenkins, J.T., Liu, P.L.-F., 2003. On two-phase sediment transport: Dilute flow. J. Geophys. Res. 108, 3057.

Ikari, H., Gotoh, H., 2023. Fully implicit discrete element method for granular column collapse. Comput. Part. Mech. 10 (2), 261–271.

Iverson, R.M., Reid, M.E., LaHusen, R.G., 1997. Debris-flow mobilization from landslides. Annu. Rev. Earth Planet. Sci. 25 (1), 85–138.

Jop, P., Forterre, Y., Pouliquen, O., 2006. A constitutive law for dense granular flows. Nature 441 (7094), 727–730.

Keetels, G.H., Chauchat, J., Breugem, W.-P., 2023. Role of turbulent kinetic energy modulation by particle–fluid interaction in sediment pick-up. J. Fluid Mech. 955, A37.

Keetels, G.H., Goeree, J.C., Van Rhee, C., 2018. Advection-diffusion sediment models in a two-phase flow perspective. J. Hydraul. Res. 56 (1), 136–140.

Kneller, B., Buckee, C., 2000. The structure and fluid mechanics of turbidity currents: a review of some recent studies and their geological implications. Sedimentology 47, 62–94.

Lee, C.-H., 2019. Multi-phase flow modeling of submarine landslides: Transformation from hyperconcentrated flows into turbidity currents. Adv. Water Resour. 131, 103383.

Lee, C.-H., 2021. Two-phase modelling of submarine granular flows with shear-induced volume change and pore-pressure feedback. J. Fluid Mech. 907, A31.

Lee, C.-H., Chen, J.-Y., 2022. Multiphase simulations and experiments of subaqueous granular collapse on an inclined plane in densely packed conditions: Effects of particle size and initial concentration. Phys. Rev. Fluids 7 (4), 044301.
Lee, C.-H., Huang, Z., 2018. A two-phase flow model for submarine granular flows: With an application to collapse of deeply-submerged granular columns. Adv. Water Resour. 115, 286–300.
Lee, C.-H., Lo, P.H.-Y., Shi, H., Huang, Z., 2022. Numerical modeling of generation of landslide tsunamis : a review. J. Earthq. Tsunami 16, 2241001.
Lee, C.-H., Low, Y.M., Chiew, Y.-M., 2016. Multi-dimensional rheology-based two-phase model for sediment transport and applications to sheet flow and pipeline scour. Phys. Fluids 28 (5), 053305.
Li, Y., Dong, Y., Chen, G., 2023. A numerical investigation of transformation rates from debris flows to turbidity currents under shearing mechanisms. Appl. Sci. 13 (7), 4105.
Lima, R.E., 2021. Estimating Changes in Fine-Sediment Storage at Eddy-Sandbars on the Colorado River, Grand Canyon, AZ Using Oblique Imagery from Remote Cameras (Ph.D. thesis). Northern Arizona University.
Lu, Y., Liu, X., Sun, J., Xie, X., Li, D., Guo, X., 2023. CFD-DEM modeling of turbidity current propagation in channels with two different topographic configurations. Front. Mar. Sci. 10, 1208739.
Mastbergen, D.R., Beinssen, K., Nédélec, Y., 2019. Watching the beach steadily disappearing: The evolution of understanding of retrogressive breach failures. J. Mar. Sci. Eng. 7 (10), 368.
Mastbergen, D.R., Van den Berg, J.H., 2003. Breaching in fine sands and the generation of sustained turbidity currents in submarine canyons. Sedimentology 50 (4), 625–637.
Mastbergen, D.R., Van den Ham, G.A., Cartigny, M., Koelewijn, A., de Kleine, M., Clare, M., Hizzett, J., Azpiroz, M., Vellinga, A., 2016. Multiple flowslide experiment in the Westerschelde Estuary, The Netherlands. In: Submarine Mass Movements and their Consequences: 7th International Symposium. Springer, pp. 241–249.
Mastbergen, D.R., Winterwerp, J.C., Bezuijen, A., 1988. On the construction of sand fill dams. Part 1: Hydraulic aspects. In: Kolkman, et al. (Eds.), Modelling Soil-Water Structure Interaction. pp. 353–362.
Meiburg, E., Kneller, B., 2010. Turbidity currents and their deposits. Annu. Rev. Fluid Mech. 42 (1), 135–156.
Meyer-Peter, E., Müller, R., 1948. Formulas for Bed-Load Transport. In: Proceedings of the 2nd Meeting of the International Association of Hydraulic Research. International Association of Hydraulic Research, IAHR, Stockholm, Sweden, pp. 39–64.
Mirza, S., Richardson, J.F., 1979. Sedimentation of suspensions of particles of two or more sizes. Chem. Eng. Sci. 34, 447–454.
Montellà, E., Chauchat, J., Bonamy, C., Weij, D., Keetels, G., Hsu, T., 2023. Numerical investigation of mode failures in submerged granular columns. Flow 3, E28. http://dx.doi.org/10.1017/flo.2023.23.
Montellà, E., Chauchat, J., Chareyre, B., Bonamy, C., Hsu, T., 2021. A two-fluid model for immersed granular avalanches with dilatancy effects. J. Fluid Mech. 925.
Mulder, T., Alexander, J., 2001. The physical character of subaqueous sedimentary density flows and their deposits. Sedimentology 48 (2), 269–299.
National-Geographic, 2018. See how sand mining threatens a way of life in Southeast Asia. Science https://www.nationalgeographic.com/science/article/vietnam-mekong-illegal-sand-mining.
Nédélec, Y., Fouine, P., Gayer, C., Collin, F., 2022. Time-lapse camera monitoring and study of recurrent breaching flow slides in Cap Ferret, France. Coasts 2 (2), 70–92.
Phan, Q.T., Bui, H.H., Nguyen, G.D., 2022. Modeling submerged granular flow across multiple regimes using the Eulerian-Eulerian approach with shear-induced volumetric behavior. Phys. Fluids 34 (6).
Richardson, J.F., Zaki, W.N., 1954. Sedimentation and fluidization: I. Trans. Inst. Chem. Eng. 32 (35), 112.
Rodi, W., 1993. Turbulence Models and Their Application in Hydraulics, a State of the Art Review, third ed. IAHR.
Rondon, L., Pouliquen, O., Aussillous, P., 2011. Granular collapse in a fluid: role of the initial volume fraction. Phys. Fluids 23, 73301.
Rowe, P., 1987. A convenient empirical equation for estimation of the Richardson–Zaki exponent. Chem. Eng. Sci. 42 (11), 2795–2796.
Savage, S.B., Babaei, M., Dabros, T., 2014. Modeling gravitational collapse of rectangular granular piles in air and water. Mech. Res. Commun. 56, 1–10.
Scholtès, L., Chareyre, B., Michallet, H., Catalano, E., Marzougui, D., 2015. Modeling wave-induced pore pressure and effective stress in a granular seabed. Contin. Mech. Thermodyn. 27, 305–323.
Sequeiros, O.E., Spinewine, B., Beaubouef, R.T., Sun, T., Garcia, M.H., Parker, G., 2010. Bedload transport and bed resistance associated with density and turbidity currents. Sedimentology 57 (6), 1463–1490.
Shademani, M., Blais, B., Shakibaeinia, A., 2021. CFD-DEM modeling of dense sub-aerial and submerged granular collapses. Water 13 (21), 2969.
Torrey, III, V.H., 1988. Retrogressive Failures in Sand Deposits of the Mississippi River. Report 2. Empirical Evidence in Support of the Hypothesized Failure Mechanism and Development of the Levee Safety Flowslide Monitoring System. Tech. Rep., Army Engineer Waterways Experiment Station Vicksburg Ms Geotechnical Lab.
Trulsson, M., Andreotti, B., Claudin, P., 2012. Transition from the viscous to inertial regime in dense suspensions. Phys. Rev. Lett. 109 (11), 118305.
Uittenboogaard, R., 1995. The importance of Internal Waves for Mixing in a Stratified Estuarine Tidal Flow (Ph.D. thesis). Delft University of Technology.
Van den Berg, J.H., Martinius, A.W., Houthuys, R., 2017. Breaching-related turbidites in fluvial and estuarine channels: Examples from outcrop and core and implications to reservoir models. Mar. Pet. Geol. 82, 178–205.
Van den Berg, J.H., Van Gelder, A., Mastbergen, D.R., 2002. The importance of breaching as a mechanism of subaqueous slope failure in fine sand. Sedimentology 49 (1), 81–95.
Van den Ham, G.A., de Groot, M.B., Mastbergen, D.R., 2014. A semi-empirical method to assess flowslide probability. In: Submarine Mass Movements and their Consequences. Springer, pp. 213–223.
Van den Ham, G.A., De Groot, M.B., Mastbergen, D.R., Van den Berg, J.H., 2022. Breaching and liquefaction in subaqueous retrogressive flow slides. Can. Geotech. J..
Van der Schrieck, G.L.M., 2012. Lecture Notes Dredging Technology. Delft University of Technology.
Van der Wal, M., 2020. Bank protection structures along the Brahmaputra-Jamuna River, a study of flowslides. Water 12 (9), 2588.
Van Dijk, W.M., Mastbergen, D.R., Van den Ham, G.A., Leuven, J.R., Kleinhans, M.G., 2018. Location and probability of shoal margin collapses in a sandy estuary. Earth Surf. Process. Landf. 43 (11), 2342–2357.
Van Rhee, C., 2001. Modelling the sedimentation process in a trailing suction hopper dredge. In: 4th Int. Conference on Multiphase Flows. New Orleans, USA.
Van Rhee, C., 2002. On the Sedimentation Process in a Trailing Suction Hopper Dredger (Ph.D. thesis). Delft University of Technology.
Van Rhee, C., 2010. Sediment entrainment at high flow velocity. J. Hydraul. Eng. 136 (9), 572–582.
Van Rhee, C., 2011. Numerical simulation of the backfilling process of a trench using a trailing suction hopper dredge. In: OMAE 2011.
Van Rhee, C., 2015. Slope failure by unstable breaching. In: Proceedings of the Institution of Civil Engineers-Maritime Engineering, Vol. 168. Thomas Telford Ltd, pp. 84–92.
Van Rhee, C., 2019. Simulation of the breaching process – experimental validation. In: Proceedings of the 22nd World Dredging Conference. Changhai, China.
Van Rhee, C., Bezuijen, A., 1998. The breaching of sand investigated in large-scale model tests. In: Coastal Engineering 1998. pp. 2509–2519.
Van Rhee, C., Talmon, A., 2010. Sedimentation and erosion of sediment at high solids concentration. In: Proceedings of the 18th International Conference on Hydrotransport. BHR Group, Cranfield, UK, pp. 211–222.
Van Rijn, L.C., 1984. Sediment pick-up functions. J. Hydraul. Eng. 110 (10), 1494–1502.
Weij, D., 2020. On the Modelling of the Unstable Breaching Process (Ph.D. thesis). Delft University of Technology.
Winterwerp, J.C., Bakker, W.T., Mastbergen, D.R., van Rossum, H., 1992. Hyperconcentrated sand-water mixture flows over erodible bed. J. Hydraul. Eng. 118 (11), 1508–1525.
Xu, W.-J., Dong, X.-Y., Ding, W.-T., 2019. Analysis of fluid-particle interaction in granular materials using coupled SPH-DEM method. Powder Technol. 353, 459–472.
Yang, G., Causon, D., Ingram, D., 1999. Cartesian cut-cell method for axisymmetric separating body flows. AIAA J. 37 (8), 905–911.
You, Y., Flemings, P., Mohrig, D., 2012. Dynamics of dilative slope failure. Geology 40 (7), 663–666.
Zhao, J., Liang, W., 2018. Multiscale modeling of large deformation in geomechanics: a coupled MPM-DEM approach. In: Proceedings of China-Europe Conference on Geotechnical Engineering: Volume 1. Springer, pp. 449–452.
Zheng, X., Pisano, F., Vardon, P.J., Hicks, M.A., 2021. An explicit stabilised material point method for coupled hydromechanical problems in two-phase porous media. Comput. Geotech. 135, 104112.